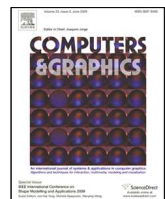




Contents lists available at ScienceDirect

## Computers &amp; Graphics

journal homepage: [www.elsevier.com/locate/cag](http://www.elsevier.com/locate/cag)

## 3D printed perforated QR codes

Jingru Yang<sup>a</sup>, Hao Peng<sup>a</sup>, Lin Liu<sup>a</sup>, Lin Lu<sup>a,\*</sup><sup>a</sup>School of Computer Science and Technology, Shandong University, Qingdao, China

## ARTICLE INFO

## Article history:

Received April 27, 2019

**Keywords:** QR Codes, Perforated, Digital Fabrication, 3D Printing

## ABSTRACT

QR codes are machine-readable optical 2D matrix barcodes which can be easily displayed physically on printed media or digitally on a screen. In recent years, artists and researchers have paid much attention to beautify and enhance QR codes with visual features beyond their plain standard format. We propose a novel method for carving a QR code on a surface in a perforated manner and fabricating it with single material via ordinary 3D printing techniques. However, it is nontrivial to directly fabricate such artistic QR codes because there are a large amount of disconnected components and small details that are difficult to be fully realized. To this end, the embedded information must be consistent and the 3D printed QR code should be readable with standard decoders, like mobile phones. With the original code, we introduce a QR evaluator to estimate its readability and then optimize the code in terms of the printability and robustness. We demonstrate the effectiveness of our techniques with a wide range of examples printed with homogeneous materials via consumer-level 3D printers.

© 2019 Elsevier B.V. All rights reserved.

## 1. Introduction

QR codes (abbreviation for Quick Response Codes)[1] are a type of machine-readable 2D matrix barcodes designed to store data efficiently. They were first applied in 1994 for the automotive industry to allow high-speed component scanning and track vehicles during manufacturing. Applications of QR codes over past decades have been broadened to product tracking, item identification, document management and general marketing (e.g. ticketing, product labeling, mobile payment systems and etc.).

QR codes become popular outside the car industry for its fast readability and increasing storage capacity. While the visual format is far from aesthetic due to pixelating by black and white squares only. Therefore, many researchers have devoted efforts to beautify the QR codes. Approaches to enhance the artistic quality of QR codes are generally grouped into two

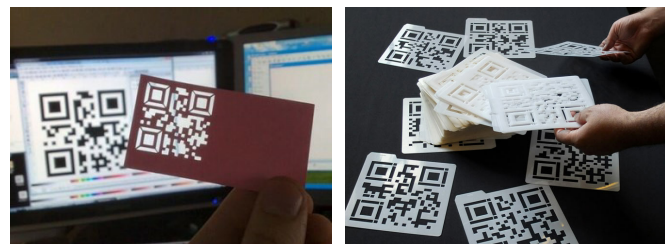


**Fig. 1. Perforated QR codes. Left: Business card by Tom Wyatt [4]; Right: Digital Nomads by Golan Levin and Asa Foster III [5].**

types: embedding images into the QR codes such as halftone QR codes [2] and stylizing modules in terms of shapes or colors like [3].

Artists design the QR codes in a perforated way and implement them by cutters, taking the material and environment as two tones for decoding, as shown in Fig. 1. Our work is inspired by this aesthetic design form, while also benefited from the emergence of 3D printing [6, 7]. We aim at carving the QR code on a surface in a perforated manner automatically and

\*Corresponding author:  
e-mail: [lulin.linda@gmail.com](mailto:lulin.linda@gmail.com) (Lin Lu)

fabricate it using single material via ordinary 3D printing techniques.

This is a challenging task due to a large amount of disconnected components, especially in high version QR codes. New connectors need to be added to make the code fabricable and enhance the stability of the 3D QR model. It is nontrivial to maintain the readability along with such manipulations on the code.

Therefore, we propose an evaluation function to quantitatively measure the readability of the manipulated QR code. The rationale is the redundancy and error correction mechanism for the QR code, i.e., a QR code has the ability to withstand certain extent of damage without information loss. For example, an artistic QR usually sacrifices its readability for enhanced visual appearance.

With this readability function, we can fulfill our goal with an optimization framework. We formulate the manipulation on the given QR code as a constrained optimization problem. Given a QR code and a target surface, we minimize the change on the code and the loss of decoding robustness and carve it on the surface in a perforated manner, with the constraints that the generated 3D QR is 3D printable, sustainable and readable by standard decoders in normal environments.

Our main contributions are:

- We propose a novel approach to automatically generate the fabricable perforated QR codes.
- We introduce an evaluation function to quantitatively measure the readability of the QR code.
- We develop an optimization framework for manipulating the QR code into a 3D printable and readable model, with minimized visual change and loss in decoding robustness.

## 2. Related work

In our work, we enhance the QR code for carving it on the surface and the model with embedded QR code is 3D printed and decoded in normal environments. In the following, we discuss works from both QR code and digital manufacturing domains in our context.

*QR-code enhancement.* In recent years, researchers have paid much attention to the modification and enhancement of QR-codes with visual features beyond their ordinary appearance [8, 9]. Cox [10] proposes an algorithm to encode binary image content as redundant numeric strings appended to the original data. Chu et al. [2] firstly combine halftone images and QR codes. They generate a binary embedding by subdividing each QR module into  $3 \times 3$  submodules to embed the halftone image and then optimize the binary pattern of each module to achieve both decoding robustness and image quality. Lin et al. [3] facilitate the process of embellishing a QR code by embedding images into a QR code using an error-aware warping technique and stylizing the black and white squares using a binary exemplar. Garateguy et al. [11] embed QR codes into color images and optimize the concentration of pixels and its corresponding luminance to minimize a visual distortion metric. Lin et al. [12] further propose a nearly real-time rendering

mechanism to improve the visual quality of QR codes while avoiding affecting their decodability.

QR-code images captured by mobile phones are usually distorted, low quality and may consist of nonuniform illumination, noise, and blur. Researchers have made significant efforts to enhance the robustness of the decoding process [13, 14, 15]. Efforts are also made to enhance the decoding capabilities and robustness of non-planar QR codes. Li et al. [16] manage to extract the finder patterns and code boundary on a cylindrical surface under the constraints that the two vertical boundaries are parallel to each other and parallel to the generatrix of the cylinder. Lay et al. [17] further lift the constraints and rectify the distortion for QR images posted on cylinders, such that the QR code can be recognized. Our carved QR codes can be scanned and decoded with mobile phone cameras in the same manner as 2D QR-codes are processed. Thus, our method has the same readability as well as camera noise and distortions as the 2D case.

*Fabrication-aware carving.* Recently, the growing popularity of personalized fabrication has motivated researchers to develop algorithms to stylize 3D shapes via creative or artistic design. Zhou et al. [18] generate single connected ornaments along curves via considering 1D pattern synthesis while constraining the topology. Dumas et al. [19] synthesize fabricable patterns along surfaces by combining structural optimization with appearance optimization. Martinez et al. [20] target the synthesis of flat shapes that are manufactured with laser cutting. Subsequently, Chen et al. [21] synthesized filigree-like structures along surfaces. They relaxed the packing problem by allowing appearance-preserving overlaps between elements. Their method produces appealing patterns, but cannot guarantee the base shape is preserved. Chen et al. [22] further propose a method for generating packed patterns on a base surface with a set of flat tiles. Zehnder et al. [23] explored the interactive design of curve networks onto surfaces, and simulated the curves as elastic rods, such that a tight packing is achieved via minimized deformations. The produced airy curve networks can be fabricated on high-end printers. These work share the same scenario that taking predefined ornamental pattern as input and performing the structure synthesis.

There are some creative researches on designing or stylizing 3D shapes to generate target images. The shadow art work [24] computes a 3D sculpture that casts several 2D shadows close to the given binary images via geometric optimizations. The perforated lampshades [25] generate continuous projected images on the wall by carving optimized distributed tiny tubes on the shell-like lampshades. More related work can be found in [7]. As far as we know, we are the first that carving the QR code on the surface, considering both fabrication constraints and QR readability.

*3D QR codes.* There are some attempts that apply QR codes in 3D objects in the context of fabrication. Li et al. [26] introduce AirCode to store data like QR-codes beneath the surface of a 3D printed object using carefully designed air pockets that can be read using computational imaging techniques. Similarly, QR codes are embedded inside 3D objects for identification purposes [27]. By taking advantage of additive layer-

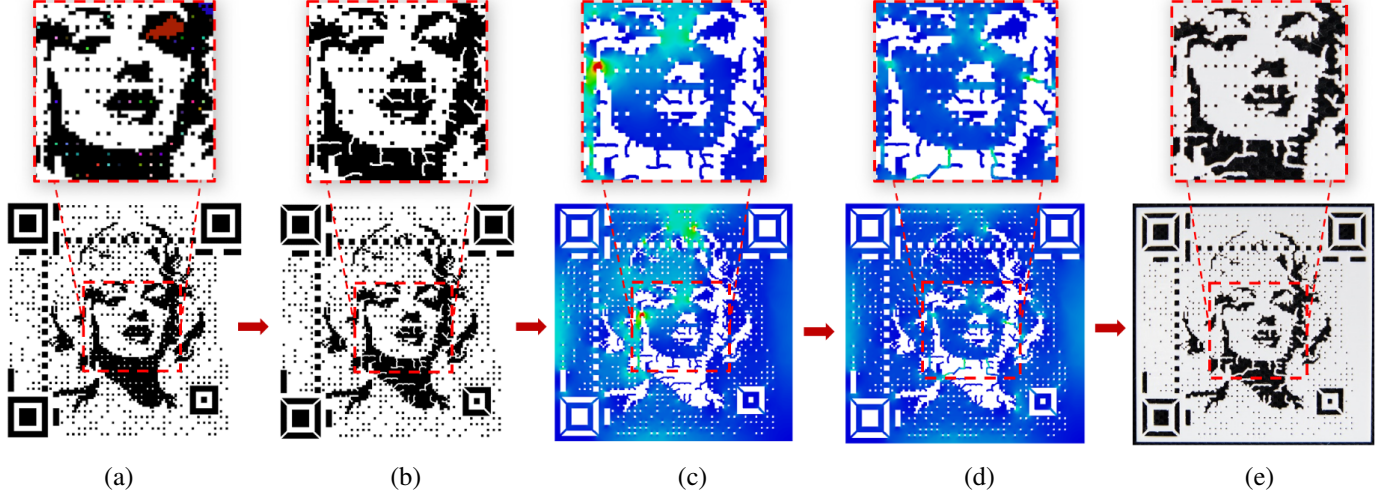


**Fig. 2.** Given a QR code and a 3D surface, our method first geometrically analyze the QR code, identifying all isolated white components (a). Then the QR code is optimized to guarantee the connectivity of all white components (b). Based on the stress analysis via FEM (c), the structural soundness is iteratively optimized by adding additional connectors while maintaining the readability of the QR code (d). The resulted 3D QR model can be 3D printed and readable by a standard decoder (e).

1 by-layer manufacturing, codes are segmented and embedded  
2 in numerous object layers without interfering with the surface.  
3 Since their pattern lies beneath the surface it suffers from low  
4 contrast and is not easily decoded without proper lighting or  
5 when printed with challenging matte materials. In contrast, our  
6 goal is to embed QR codes with robust readability and mini-  
7 mal geometry distortion. Wei et al. [28] embed QR codes for  
8 anti-counterfeiting utilizing SLM-based 3D printing. The QR  
9 is fabricated with a specific “tagging” material such that it can  
10 be recognized via X-ray imaging. Recently Kikuchi et al. [29]  
11 suggested an embedding of QR codes onto CAD models repre-  
12 sented by B-spline surfaces. In contrast, our method is not lim-  
13 ited to only CAD models or B-spline representations but may  
14 be applied in a general manner to various models.

### 15 3. Overview

16 Given an artistic QR code and a target surface, we aim at  
17 carving the code on the surface in a perforated manner, such  
18 that the QR-embedded model can be 3D printed and decoded  
19 by standard decoders in normal environments. The resulting 3D  
20 QR code should satisfy the connectivity, structural soundness,  
21 and decoding robustness. We minimize the visual change of the  
22 QR code with all these constraints.

23 Taking an input artistic QR code image  $I$  (Fig. 2a), we extract  
24 the embedded QR matrix  $Q$ , and recover its original symbol  $Q_0$   
25 via the Reed Solomon algorithm. Then we regard  $Q_0$  as the  
26 baseline of the QR code and propose a loss function to quan-  
27 titatively measure the decoding robustness of the manipulated  
28 QR code.

29 We perform a two-stage optimization on the QR code, a con-  
30 nectivity optimization stage to guarantee the printability, and a  
31 structure optimization stage to make sure the printed model is  
32 sustainable.

33 We set the black modules in the QR code as the negative part  
34 to be carved out, and the white modules as the positive part

35 that are fabricated in solid. Thus, the white modules must be  
36 connected in one piece, otherwise the 3D QR model cannot be  
37 fully fabricated. The connectivity optimization first analyzes  
38 all white components, and then adds the minimal amount of  
39 additional connectors between isolated white components such  
40 that all solids connect, considering the readability loss. We em-  
41 ploy the minimum spanning tree algorithm to iteratively add the  
42 connector until all white modules form one single component  
43 (Fig. 2b).

44 To guarantee that the perforated model is stable and sustain-  
45 able, we further optimize the 3D QR code on the surface based  
46 on structural analysis. We basically follow the standard work-  
47 flow of structural optimization, except that the QR readability  
48 function is fully involved. We first obtain the stress map and  
49 displacement map of the 3D QR model under given forces via  
50 finite element methods (FEM) (Fig. 2c). We propose a weight  
51 computation criteria based on both the distance and readabil-  
52 ity loss to evaluate the cost of the connector. Then the stability  
53 of the whole QR code is iteratively enhanced by adding con-  
54 nectors between the weak region and its neighboring part with  
55 the minimal cost (Fig. 2d). For each iteration, the readability is  
56 evaluated and guaranteed.

57 Finally, we obtain the fabricable 3D perforated QR code with  
58 both structural soundness and decoding robustness (Fig. 2e).

### 59 4. QR codes evaluation

60 In this section, we introduce an evaluation function to quan-  
61 titatively measure the readability of the QR code.

#### 62 4.1. Preliminaries on QR codes

63 A standard QR code is an  $n \times n$  square matrix, which con-  
64 tains amounts of black and white squares called modules. Each  
65 module  $m$  denotes a bit of data, and  $m = \{0, 1\}$  when the mod-  
66 ule color is black and white, respectively. The QR code sym-  
67 bol is classified into 40 versions according to the number of

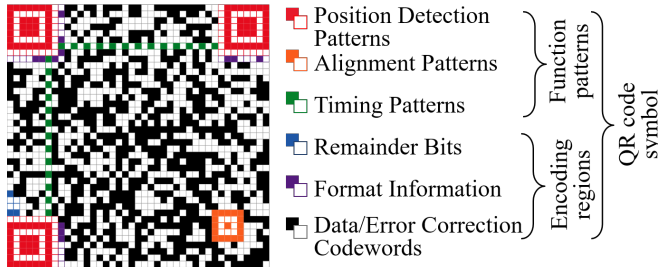


Fig. 3. Structure of a QR code symbol.

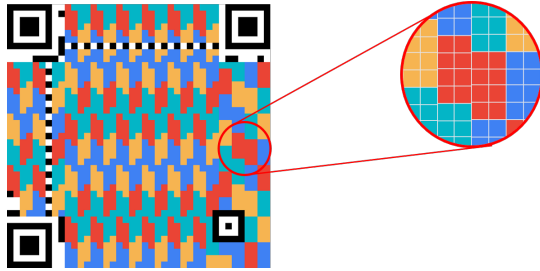


Fig. 4. A version 6, high error correction level QR code has 4 blocks highlighted by different colors.

modules, i.e., a QR code of version  $V = 1, \dots, 40$  includes  $(17 + 4 \times V)^2$  modules. The QR code symbol is designed to have the error correction capability and redundancy to recover data when damaged. It has four levels for error correction: *Low*, *Medium*, *Quartile* and *High* that support 7%, 15%, 25% and 30% recovery capacity, respectively.

The structure of a QR code symbol (Fig. 3) takes the form of two parts, the *function patterns* and *encoding regions*.

The function patterns play a pivotal role in the positioning and recognition of QR codes. They include: *position detection patterns* used to recognize QR code and identify QR version; *timing patterns*, enabling module coordinates in the symbol to be determined; and *alignment patterns* used to correct QR code distortions.

The encoding regions contain *data/error correction codewords*, the *version region* (if  $V > 6$ ), the *format information* and *remainder bits* as necessary.

With regard to the region of data/error correction codewords, it is split into several *blocks* depending on the symbol version and error correction level (see Fig. 4). The data is evenly distributed among each block  $B$ , and then the block exploits the Reed Solomon algorithm [1] to generate a series of error correction codewords placed after the data codeword sequence. Each *codeword*  $C$  in data/error correction codewords is formed by eight neighboring modules together. A defect converting one module from dark to light or vice versa will result in the affected symbol character misdecoding as an apparently valid but different codeword. Such error causes a substitution error in the data and requires two error correction codewords to correct it. For withstanding damage without loss of data, the *maximum number of erroneous codewords*  $r$  must be less than half of the error correction codewords number per block.

In general, a QR code symbol has four format regions to pro-

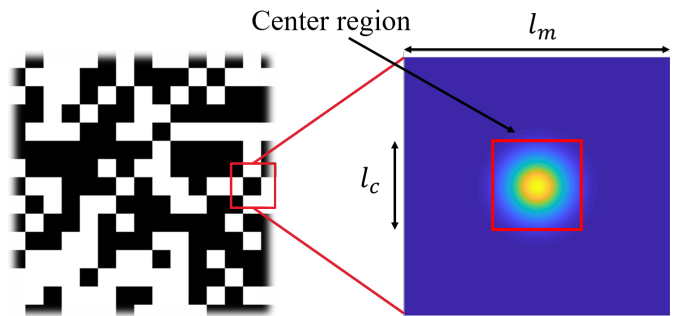


Fig. 5. Left: A module in QR code highlighted in red. Right: Diagram of this module showing possible sampling points hit in it and its center region using the Gaussian function.

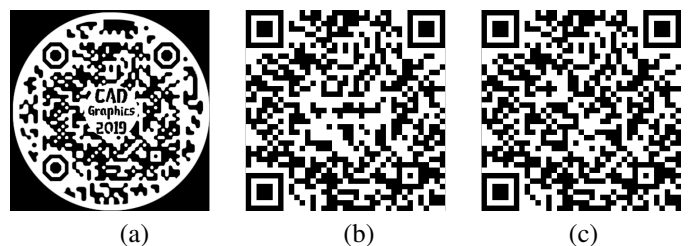


Fig. 6. (a) Input artistic QR code image; (b) the QR code  $Q$  extracted from the input; (c) the original QR code  $Q_0$  recovered from  $Q$ .

vide sufficient redundancy. Each format region  $F$  is a set of neighboring modules (see Fig. 3, format regions are highlighted in purple). Similar to the codeword, format region  $F$  will be damaged by any erroneous of a module. The remainder bits padded into the encoding region do not carry information, just to fill data codeword capacity of the symbol when necessary.

#### 4.2. QR codes recovery

Taking an artistic QR code image  $I$  as input, we first binarize the image and then take an open source library Zxing [30] to detect the *position detection patterns* and *alignment patterns* of QR code. The position detection pattern can be recognized easily for it construes a dark-light-dark-light-dark sequence the relative widths of each module of which are in the ratios 1:1:3:1:1.

Once all position detection patterns identified, we measure the module width  $l_m$  via drawing parallel lines and then extract the module matrix in the QR code region. To safely extract module matrix, Lin et al. [3] suggest drawing a center region for each module that contains the correct information. The width of the center region  $l_c$  shall be at least 1/3 of module width (Fig. 5). A Gaussian distribution of sampling points proposed in [11] is adopted to address this requirement and then we extract the QR matrix by sampling on a grid (Fig. 6b).

Let  $Q$  be the QR module matrix extracted from the input QR image. We recover the original QR code  $Q_0$  from  $Q$ , which is regarded as the baseline of  $Q$  via Reed Solomon algorithm [1] (Fig. 6c).

#### 4.3. Loss of QR readability

We define  $L(Q)$  as the loss of QR readability caused by the difference between  $Q$  and  $Q_0$ . Specifically, only errors occur in

the data/error correction codewords or the format regions could affect QR code readability as reported on the QR standard documents. Let  $\Delta Q$  denote QR code errors. The loss of QR readability  $L(Q)$  can be described as a total loss of data/error correction capability  $L_C$  and format regions redundancy  $L_F$ :

$$L(Q) = L_C + L_F. \quad (1)$$

We denote each codeword in the form of  $C = \{m_i\}_{i=1}^8$  and define  $\Delta C$  as an indicator function to indicate whether  $C$  is erroneous or not.  $\Delta C = 1$  indicates the total square deviation of this codeword  $\sum_{i=1}^8 \Delta m_i^2 > 0$ , otherwise  $\Delta C = 0$ . In order to measure the loss caused by the erroneous codewords, we formulate the loss function of data/error correction codewords  $L_c$  as:

$$L_C = \begin{cases} \frac{1}{n_B} \sum_{i=1}^{n_B} \left( \frac{1}{r} \sum_{j=1}^{n_C} \Delta C_{ij} \right)^2, & \forall B_i \subset Q, \sum_{j=1}^{n_C} \Delta C_{ij} \leq r \\ \infty, & \exists B_i \subset Q, \sum_{j=1}^{n_C} \Delta C_{ij} > r \end{cases} \quad (2)$$

where  $n_B$  is the number of blocks, and each block has  $n_C$  codewords. Here we propose a min-max normalization for each block to scale the loss per block in  $[0, 1]$  and  $L_C$  is to be infinity if the error number of a block exceeds  $r$ .

Let  $\Delta F$  be an indicator of whether this format region is damaged ( $= 1$ ) or not ( $= 0$ ). Let  $\Delta F = 1$  when the total square deviation of  $F \sum_{m_i \in F} \Delta m_i^2 > 0$ , while  $\Delta F = 0$  when  $\sum_{m_i \in F} \Delta m_i^2 = 0$ .

To guarantee QR code readability, the damage on format regions needs to be as little as possible and at least one format region cannot be changed. Thus, we formulate the loss of format regions redundancy  $L_F$  as:

$$L_F = \begin{cases} \frac{1}{4} \sum_{i=1}^4 \Delta F_i, & \sum_{i=1}^4 \Delta F_i < 4 \\ \infty, & \sum_{i=1}^4 \Delta F_i = 4 \end{cases} \quad (3)$$

Therefore, the loss of QR readability  $L(Q)$  can be computed by Eqn. 2 and 3.

## 5. QR codes optimization

We propose a two-stage optimization to automatically generate the connected and stable perforated QR codes.

### 5.1. Connectivity optimization

To ensure perforated QR codes printability, a connectivity optimization algorithm shall be put forward to connect whole white components into a single component. Otherwise, the isolated white regions suspending in the void lead to a printing failure.

We divide the connectivity optimization into two steps based on the QR code structure. For function patterns, we follow the diagonal design done by the artist as shown in Fig. 1 to make the white components connected (Fig. 7). For encoding regions, we build an iterative optimization algorithm to connect the isolated white components.

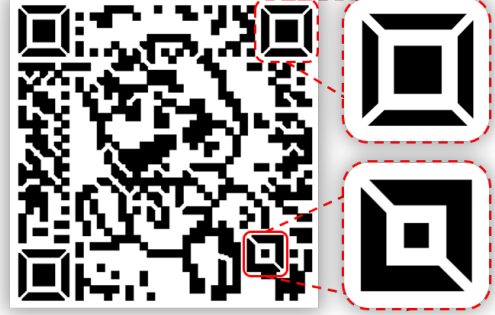


Fig. 7. The connectivity treatment for the position detection patterns and alignment patterns.

A straightforward way to obtain a single connected image is to link among isolated white components via minimal Euclidean distance using the spanning tree algorithm. It makes the minimum change on the visual appearance of the QR code. However, this may cause decoding failures or decrease the decoding robustness. To ensure the readability, the effect on the QR codes error correction capabilities must be considered. Therefore, we consider both Euclidean distance and the cost of QR codes error correction capabilities in the connectivity optimization on the encoding regions. Given a QR image  $I$ , we label all white components  $\{S_i\}_{i=1}^N$ . Let  $p$  and  $q$  be the points on the contours of  $S_i$  and  $S_j$  respectively. Then we formulate the weight  $w_{ij}$  between  $S_i$  and  $S_j$  as:

$$w_{ij} = \min_{p,q} (\lambda L(Q) + \|p - q\|^2), \quad (4)$$

where  $L(Q)$  is defined in Sec. 4.3, indicating the loss on the readability when adding the connector between  $p$  and  $q$ ,  $\lambda$  is the weight parameter for the readability.

We note that there is no need to compute weights of all white component pairs. For each point  $p \in S_i$ , we just cast its 2D visible region  $V_p$  and calculate the weight of  $p$  and  $q \in V_p \cap S_j$  to reduce the computational cost. Then we randomly pick out a white component and connect its neighbor with the minimal weight iteratively until all white components are connected.

Fig. 8 shows an example on connectivity optimization, together with the comparison result using the shortest Euclidean distance path. The change of the readability loss value is plotted in Fig. 9. The loss value increases along with the iterations. However, it goes to infinity value if only considering the distance in generating the connectors, causing the QR code non-decodable.

### 5.2. Structural optimization

We first carve the QR code on the surface and generate the mesh. Specifically, we project the optimized QR code image from Sec. 5.1 on the surface with target QR position defined by users. We assume that the carving region is continuous, with no self occlusions and that the projection direction is in the normal direction to the surface as QR codes are typically scanned from top-view. The projected QR image on the surface defines a partition of the surface vertices inside the QR region into black and

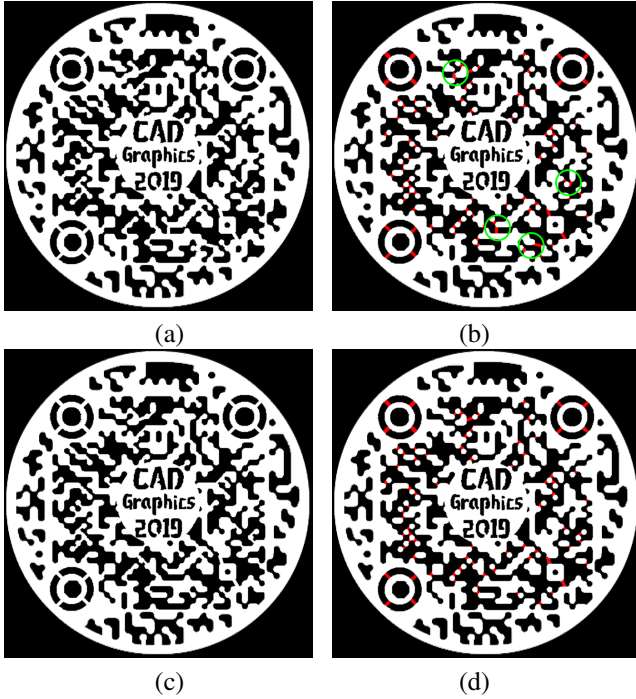


**Fig. 8.** (a) The connectivity enforcement by minimal Euclidean distance without considering the QR readability ( $\lambda = 0$  in Eqn. 4) cannot be decoded. The new connectors are highlighted in red (b). (c) The connectivity optimization result considering the QR readability ( $\lambda = 1$  in Eqn. 4) with new connectors highlighted in red (d). The green circle marks the difference between (b) and (d). The input QR code is in Fig. 6.

white modules. The black modules are hollowed out as the negative part and white modules are the remaining solid. Note that we remesh the QR region, i.e., white modules, on the surface into a dense set of triangles.

Then we perform the static analysis via FEM on the shell model, in which the shell thickness is taken as a parameter. We fix the QR boundaries as the boundary condition and apply uniform pressure on each face along its normal direction. The stress map and displacement map of the QR code are obtained for the optimization.

Similar to connectivity optimization, both distance and the cost of QR readability shall be considered. In particular, the new connector should comprise the shortest connecting path and cause the minimum readability loss. Refer to Fig. 10, end-

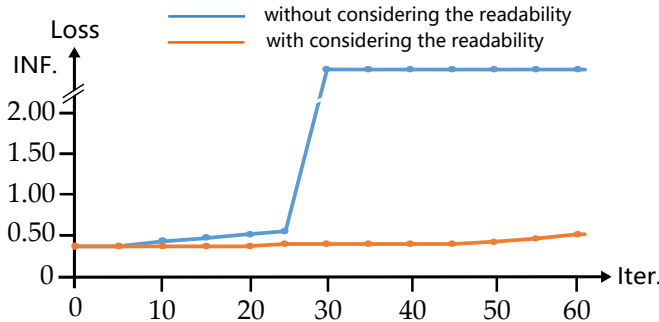


**Fig. 9.** The readability loss along with the connectivity optimization iterations.

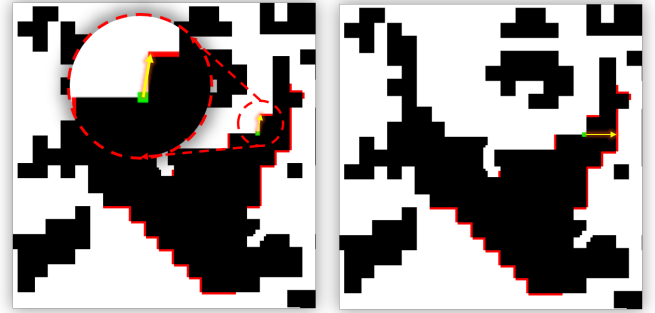


**Fig. 10.** Selection of the connectors in structural optimization. The starting point is marked green, all possible connecting points are marked red and the yellow line is the connector with the shortest path. Left: only the Euclidean distance is adopted; Right: both Euclidean and geodesic distance are adopted.

points of the new connector should be on the boundary of the white component and cross the black component. It is clear that the Euclidean distance is not enough to evaluate the cost of the connector (Fig. 10a). Intuitively, a good connector is made by two points with the shortest path in Euclidean distance, but the largest path in geodesic distance (Fig. 10b).

Therefore, we propose a criteria for the connectors based on both the distance and readability loss to evaluate the cost of the connector as follows. The connector by points  $p$  and  $q$  has the cost  $c_{pq}$ :

$$c_{pq} = \lambda L(Q) + \frac{\|p - q\|^2}{\|p, q\|_g}, \quad (5)$$

where  $\|p, q\|_g$  indicates the geodesic distance between  $p$  and  $q$ .

In the structural optimization, we pick the point with the largest deformation after the FEM analysis and add the connector from this point to the other with the smallest cost defined in Eqn. 5. Then we update the model and perform FEM until the whole model is free of weak regions, i.e., all stress is below the yielding stress value  $\chi$ . In our experiments,  $\chi = 10MPa$  for the PLA material. The detailed algorithm is given in Alg. 1.

Fig. 11 shows an example of structural optimization, in which the physical size of the QR code is  $12 \times 12$ cm, the thickness is 0.5cm and the pressure on each face is 5Pa.

## 6. Results and discussions

We implemented our approach in C++ on an Intel Core™ i7-7700K CPU@4.0GHz and 16GB RAM. We use OpenCV library [31] for image processing, CGAL [32] for mesh manipulation, and Abaqus Unified FEA for stress analysis in the implementation.

We show the input QR codes, the optimized codes and 3D printed results of the carving QR codes in Fig. 15. The models are fabricated by an FDM-based printer (HORI Z500) with white PLA material, whose nozzle diameter is 0.4mm. Statistics of the results including QR resolution and version, printing size, running time and the number of iterations are listed in Tab. 1.

As shown in Tab. 1, both connectivity optimization and structural optimization perform well for different versions of QR

**Algorithm 1** Structural optimization on the perforated QR.

---

**Input:** The perforated model  $M$ , yielding stress value  $\chi$ ;  
**Output:** The optimized model;

- 1: Compute the stress map  $\sigma$  and strain map  $\epsilon$  of  $M$  via FEM;
- 2: **while**  $\sigma_{max} > \chi$  **do**
- 3:   Find maximum strain point  $p$ ,  $c_{min} \leftarrow \infty$ ;
- 4:   Compute visible points  $V_p$  of  $p$  on the white contour;
- 5:   **for**  $q \in V_p$  **do**
- 6:     Compute  $c_{pq}$  following Eqn. 5;
- 7:     **if**  $c_{pq} < c_{min}$  **then**
- 8:        $c_{min} \leftarrow c_{pq}$ ;
- 9:     **end if**
- 10:   **end for**
- 11: **if**  $c_{min} = \infty$  **then**
- 12:    **return** the current model;
- 13: **end if**
- 14:   Connect line  $pq$  where  $c_{pq} = c_{min}$ , update  $M$ ,  $\sigma$  and  $\epsilon$ ;
- 15: **end while**
- 16: **return** the stable model  $M$ .

---

1 codes. Especially, our algorithm works for the artistically enhanced QR codes generated by previous work. For connectivity optimization, the number of iterations is determined by the number of isolated white regions. It takes the Einstein code 493 iterations for generating the single connected white region due to a large number of fractures for the halftone effect. For structural optimization, the number of iterations corresponds to the structure of the QR code. Since the entire QR code needs to be evaluated to update the loss in each iteration, the time for each iteration is similar. The loss evaluation is also the most time-consuming part in the optimization, which relates to the given QR resolution.

13 To validate the readability of the fabricated carving QR  
14 codes, we designed and completed four experiments to evaluate  
15 the robustness of our QR codes. We regard a decoding as  
16 a successful one if the QR code is decoded within 2 seconds.

17 First, we use different mainstream mobile devices standard  
18 QR readers to test the decoding success rate of QR codes under  
19 the black background. If the decoding is successful, we mark it  
20 with  $\checkmark$ , otherwise we mark it with  $\times$  in Tab. 2. It can be seen  
21 from the data in Tab. 2 that carving QR codes can be decoded  
22 successfully by mainstream decoders and mobile phones.

23 Second, we validate the readability of the fabricated QR  
24 codes over different background colors. We scan each QR  
25 code 20 times in Fig. 15 under six specific background colors  
26 (red, green, blue, cyan, magenta, yellow), 120 times for  
27 each color. The corresponding success rate are 95.8%, 96.7%,  
28 98.3%, 95.8%, 97.5% and 94.2% for the six background colors,  
29 respectively. As the QR codes are all printed in white materials,  
30 dark background colors indicate high contrast and thus raise  
31 the successful rate. Fig. 12 shows the Mario QR code in three  
32 background colors can all be successfully decoded.

33 Third, we tested our method on different printing materials.  
34 Our method is friendly to various materials as long as the  
35 printed and background color produce enough contrast. Fig. 13  
36 shows the Mario model in different colors of the PLA material,

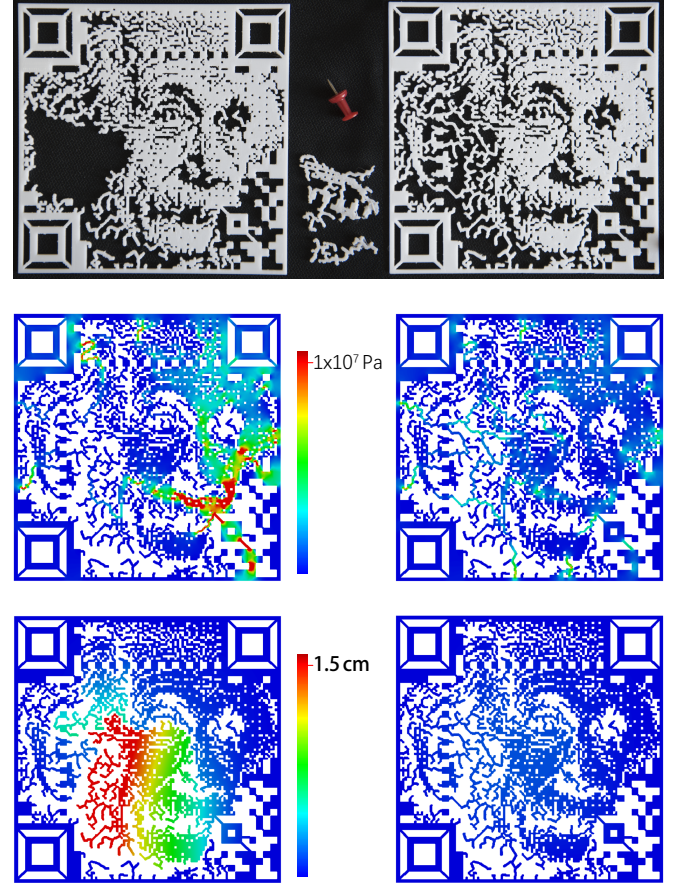


Fig. 11. First row: the 3D printed QR code without structural optimization (left) and with structural optimization (right). The second row shows the related stress map and the third row shows the related displacement map.

which can all be easily decoded.

Finally, we tested the robustness of the printed QR codes to different scanning angles. For the Einstein QR code, we scan both the input QR image and the perforated QR code on the cuboid by Mi8 Scanner 20 times from a range of scanning angles and list the average statistics in Fig. 14. It shows that the original input QR codes possess robustness within 30 degrees tilt from the orthogonal direction to QR codes. There is a clear reducing trend of decoding success rate with the increase of the scanning angle. Especially the QR codes cannot be decoded when the tilt angle is greater than 60 degrees. Comparing to the original QR code, our 3D printed carving QR code allows smaller tilt, which has good robustness within 20 degrees of tilt.



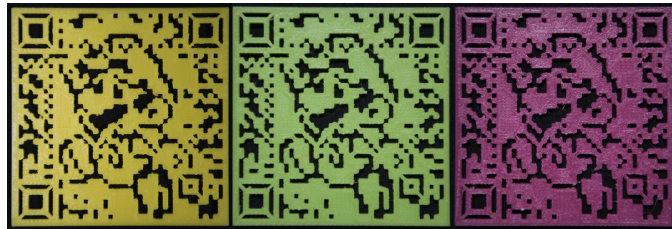
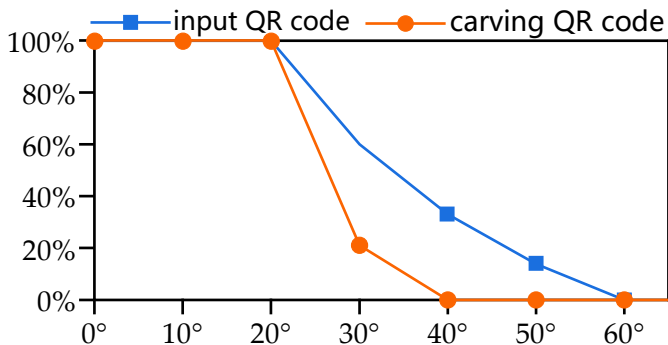
Fig. 12. Perforated QR models in different background colors can be decoded.

**Table 1. Statistics of the results.**

Model	QR Image	Resolution	QR Version	Printed QR size (cm)	Connectivity Optimization time(s) & #Iter.	Structural Optimization time(s) & #Iter.
Cuboid	Flower	700x700	8	14x14x0.2	842 & 140	387 & 7
Cuboid	Monroe	640x640	6	13x13x0.2	456 & 79	156 & 3
Cuboid	Einstein	600x600	5	12x12x0.2	2465 & 493	588 & 12
Cuboid	Mario	260x260	6	5x5x0.2	179 & 35	232 & 6
Cuboid	CADGraphics	370x370	5	9x9x0.2	336 & 61	168 & 4
Bunny				18.9x18.2x14.6		

**Table 2. Readability test on different decoders.**

	Flower	Monroe	Einstein	Mario	CADGraphics (Cuboid)	CADGraphics (Bunny)
iPhone & QuickMark	✓	✓	✓	✓	✓	✓
iPhone & NeoReader	✓	✓	✓	✓	✗	✗
Samsung & WeChat	✓	✓	✓	✓	✓	✓
Mi8 & Scanner	✓	✓	✓	✓	✓	✓
Huawei & Huawei Vision	✓	✓	✓	✓	✓	✓

**Fig. 13. Perforated QR models printed in different colors can be decoded.****Fig. 14. Robustness on the scanning angles for the Einstein QR code.**

It is difficult to decode successfully when the tilt angle is greater than 30 degrees. The reason is that the sidewall introduces self-occlusion to QR code. We remark that the CADGraphics code on the Bunny model needs to be scanned from the top view.

## 7. Conclusion and future work

In this paper, we introduce a method for manipulating the QR code into a 3D printable and readable model, with minimized visual change and loss of decoding robustness. We propose a significant QR code evaluator to evaluate the loss of QR readability throughout the whole optimization, which is used to en-

sure readability. Then we discuss two major optimization components to obtain the fabricable carving QR code with structural soundness automatically. One is the connectivity optimization to make sure that the QR code is printable and decoding robustness. The other is the structural optimization to generate decodable and stable 3D carving QR code. Finally, we validated the effectiveness of our method on a series of QR codes and evaluate the robustness of the resulting QR codes in various aspects.

For the future work, we would like to investigate on the perforated QR code on disconnected regions. Exploring the functionalities of the 3D printed QR code is also interesting.

## Acknowledgments

We thank the reviewers for their valuable suggestions. This work is supported by NSFC (61572291) and Young Scholars Program of Shandong University (YSPSDU).

## References

- [1] Wave, D. Information technology automatic identification and data capture techniques qr code bar code symbology specification. International Organization for Standardization, ISO/IEC 2015;18004.
- [2] Chu, HK, Chang, CS, Lee, RR, Mitra, NJ. Halftone qr codes. ACM Trans Graph 2013;32(6):217:1–217:8. URL: <http://doi.acm.org/10.1145/2508363.2508408>. doi:10.1145/2508363.2508408.
- [3] Lin, YS, Luo, SJ, Chen, BY. Artistic qr code embellishment. Computer Graphics Forum 2013;32(7):137–146. URL: <https://onlinelibrary.wiley.com/doi/abs/10.1111/cgf.12221>. doi:10.1111/cgf.12221. arXiv:<https://onlinelibrary.wiley.com/doi/pdf/10.1111/cgf.12221>.
- [4] Wyatt, T. qr code business card. 2008. URL: <https://www.flickr.com/photos/fucksocks/2425729926>.
- [5] Levin, G, III, AF. Qr codes for digital nomads. 2011. URL: <http://www.flong.com/projects/qr-codes-for-digital-nomads/>.
- [6] Bo, Z, Lu, L, Sharf, A, Xia, Y, Deussen, O, Chen, B. Printable 3d trees. 2017. URL: <https://onlinelibrary.wiley.com/doi/abs/10.1111/cgf.13269>. doi:10.1111/cgf.13269. arXiv:<https://onlinelibrary.wiley.com/doi/pdf/10.1111/cgf.13269>.

- [7] Bernd, B, Paolo, C, Luigi, M, Nico, P. State of the art on stylized fabrication. Computer Graphics Forum 2018;0(0). URL: <https://onlinelibrary.wiley.com/doi/abs/10.1111/cgf.13327>. doi:10.1111/cgf.13327. arXiv:<https://onlinelibrary.wiley.com/doi/pdf/10.1111/cgf.13327>.
- [8] Visualead, . Visualead: Visual qr code generator. 2019. URL: <http://www.visualead.com/>.
- [9] FLICKR, . Qr code art. <http://www.flickr.com/groups/qr-art/>; 2009.
- [10] Cox, R. Qart codes. <http://research.swtch.com/qart>; 2012.
- [11] Garateguy, GJ, Arce, GR, Lau, DL, Villarreal, OP. Qr images: Optimized image embedding in qr codes. IEEE Transactions on Image Processing 2014;23(7):2842–2853. doi:10.1109/TIP.2014.2321501.
- [12] Lin, SS, Hu, MC, Lee, CH, Lee, TY. Efficient qr code beautification with high quality visual content. IEEE Transactions on Multimedia 2015;17(9):1515–1524. doi:10.1109/TMM.2015.2437711.
- [13] Chu, CH, Yang, DN, Chen, MS. Image stablization for 2d barcode in handheld devices. In: Proceedings of the 15th ACM International Conference on Multimedia. MM '07; New York, NY, USA: ACM. ISBN 978-1-59593-702-5; 2007, p. 697–706. URL: <http://doi.acm.org/10.1145/1291233.1291394>. doi:10.1145/1291233.1291394.
- [14] Yang, H, Kot, AC, Jiang, X. Binarization of low-quality barcode images captured by mobile phones using local window of adaptive location and size. IEEE Transactions on Image Processing 2012;21(1):418–425. doi:10.1109/TIP.2011.2155074.
- [15] van Gennip, Y, Athavale, P, Gilles, J, Choksi, R. A regularization approach to blind deblurring and denoising of qr barcodes. IEEE Transactions on Image Processing 2015;24(9):2864–2873. doi:10.1109/TIP.2015.2432675.
- [16] Li, X, Shi, Z, Guo, D, He, S. Reconstruct argorithm of 2d barcode for reading the qr code on cylindrical surface. In: 2013 International Conference on Anti-Counterfeiting, Security and Identification (ASID). 2013, p. 1–5. doi:10.1109/ICASID.2013.6825309.
- [17] Lay, KT, Wang, LJ, Han, PL, Lin, YS. Rectification of images of qr codes posted on cylinders by conic segmentation. In: 2015 IEEE International Conference on Signal and Image Processing Applications (ICSIPA). 2015, p. 389–393. doi:10.1109/ICSIPA.2015.7412222.
- [18] Zhou, S, Jiang, C, Lefebvre, S. Topology-constrained synthesis of vector patterns. ACM Trans Graph 2014;33(6):215:1–215:11. URL: <http://doi.acm.org/10.1145/2661229.2661238>. doi:10.1145/2661229.2661238.
- [19] Dumas, J, Lu, A, Lefebvre, S, Wu, J, Dick, C. By-example synthesis of structurally sound patterns. ACM Trans Graph 2015;34(4):137:1–137:12. URL: <http://doi.acm.org/10.1145/2766984>. doi:10.1145/2766984.
- [20] Martínez, J, Dumas, J, Lefebvre, S, Wei, LY. Structure and appearance optimization for controllable shape design. ACM Trans Graph 2015;34(6):229:1–229:11. URL: <http://doi.acm.org/10.1145/2816795.2818101>. doi:10.1145/2816795.2818101.
- [21] Chen, C, Huang, W, Zhou, B, Liu, C, Mow, WH. Pi-code: A new picture-embedding 2d barcode. Trans Img Proc 2016;25(8):3444–3458. URL: <https://doi.org/10.1109/TIP.2016.2573592>.
- [22] Chen, W, Ma, Y, Lefebvre, S, Xin, S, Martínez, J, wang, w. Fabricable tile decors. ACM Trans Graph 2017;36(6):175:1–175:15. URL: <http://doi.acm.org/10.1145/3130800.3130817>. doi:10.1145/3130800.3130817.
- [23] Zehnder, J, Coros, S, Thomaszewski, B. Designing structurally-sound ornamental curve networks. ACM Trans Graph 2016;35(4):99:1–99:10. URL: <http://doi.acm.org/10.1145/2897824.2925888>. doi:10.1145/2897824.2925888.
- [24] Mitra, NJ, Pauly, M. Shadow art. ACM Trans Graph 2009;28(5):156:1–156:7. URL: <http://doi.acm.org/10.1145/1618452.1618502>. doi:10.1145/1618452.1618502.
- [25] Zhao, H, Lu, L, Wei, Y, Lischinski, D, Sharf, A, Cohen-Or, D, et al. Printed perforated lampshades for continuous projective images. ACM Trans Graph 2016;35(5):154:1–154:11. URL: <http://doi.acm.org/10.1145/2907049>. doi:10.1145/2907049.
- [26] Li, D, Nair, AS, Nayar, SK, Zheng, C. Aircode: Unobtrusive physical tags for digital fabrication. In: Proceedings of the 30th Annual ACM Symposium on User Interface Software and Technology. UIST '17; 2017, p. 449–460.
- [27] Chen, F, Luo, Y, Tsoutsos, NG, Maniatakis, M, Shahin, K, Gupta, N. Embedding tracking codes in additive manufactured parts for product authentication. Advanced Engineering Materials 2018;0(0):1800495. URL: <https://onlinelibrary.wiley.com/doi/abs/10.1002/adem.201800495>. arXiv:<https://onlinelibrary.wiley.com/doi/pdf/10.1002/adem.201800495>.
- [28] Wei, C, Sun, Z, Huang, Y, Li, L. Embedding anti-counterfeiting features in metallic components via multiple material additive manufacturing. Additive Manufacturing 2018;24:1 – 12. URL: <http://www.sciencedirect.com/science/article/pii/S2214860418305189>. doi:<https://doi.org/10.1016/j.addma.2018.09.003>.
- [29] Kikuchi, R, Yoshikawa, S, Jayaraman, PK, Zheng, J, Maekawa, T. Embedding qr codes onto b-spline surfaces for 3d printing. Computer-Aided Design 2018;102:215 – 223. URL: <http://www.sciencedirect.com/science/article/pii/S0010448518302537>. doi:<https://doi.org/10.1016/j.cad.2018.04.025>; special Issue on SPM 2018.
- [30] Owen, S, et al. zxing-multi-format 1d/2d barcode image processing library with clients for android, java. Github 2014;.
- [31] Open source computer vision library. <https://github.com/opencv>; 2015.
- [32] The CGAL Project, . CGAL User and Reference Manual. 4.12 ed.; CGAL Editorial Board; 2018. URL: <https://doc.cgal.org/4.12/Manual/packages.html>.



**Fig. 15.** (a) Input artistic QR code. (b) The optimized QR code, in which the connectors introduced in connectivity optimization are highlighted in red, connectors introduced in structural optimization are highlighted in green. (c) 3D printed QR code. The Flower, Monroe, and Einstein in the first three rows are generated by [2]. The Mario code is generated by [10]. The original pictures in the first four QR codes are from <https://project-tideas.com/famous-clipart-patterns.html> and <https://www.shutterstock.com/image-vector/>. The CADGraphics code is generated by <https://www.unitag.io/qrcode>.